# High Resolution DNS of Incompressible Homogeneous Forced Turbulence –Time Dependence of the Statistics–

Takashi Ishihara and Yukio Kaneda

Nagoya University, Nagoya 464-8603, JAPAN

**Abstract.** Results of direct numerical simulation (DNS) of incompressible homogeneous and isotropic forced turbulence with grid points up to $1024^3$ are presented with emphasis on the time dependence of the turbulence statistics. The Taylor micro scale Reynolds number at a quasi-stationary state is 283 in the DNS with $1024^3$ grid points, and the energy spectrum exhibits an universal equilibrium range. The results suggest that for $R_\lambda > 280$ or so, the energy dissipation rate normalized by the integral length scale and root-mean-square velocity is almost independent of $R_\lambda$ and is $0.44 - 0.45$.

## 1 Introduction

Direct numerical simulation (DNS) of turbulence provides us with detailed data of turbulence statistics free from experimental uncertainties, under well controlled conditions. DNS can therefore be a powerful means not only for direct applications for practical problems, but also for the understanding of basic features of turbulence dynamics. In DNS for the latter purpose, a key role is played by the idea that the turbulence statistics at sufficiently small scales are universal in the sense that they are insensitive to the details of the initial and boundary conditions, and the external forcing at large scales, provided that the Reynolds number is sufficiently high. This idea is in accordance with the Kolmogorov hypothesis [1], and has been supported by experiments and simulations. This idea also implies that for the understanding of the universal feature of small scale statistics in turbulence, it is desirable to simulate turbulence at Reynolds number as high as possible, and that such features may be captured by DNS under simple boundary and forcing conditions. It is then reasonable to use very simple boundary conditions such as periodic boundary conditions, particularly because the number of the degrees of freedom to be treated in DNS of turbulence increases rapidly with the Reynolds number so that the use of complicated boundary conditions would result in heavier computation.

There have been in fact extensive studies of turbulence based on DNS using such simple conditions, as seen in Fig.1, which shows a rough sketch (of course not complete) of the history of the DNS of homogeneous isotropic incompressible turbulence obeying the Navier-Stokes equations under periodic boundary conditions. Since the pioneering work by Orszag in 1969[2], in DNS of which the number of grid points was $32^3$, the number has been increasing approximately exponentially in time, and now becomes over $1024^3$, as seen in Fig. 1 [3–7].

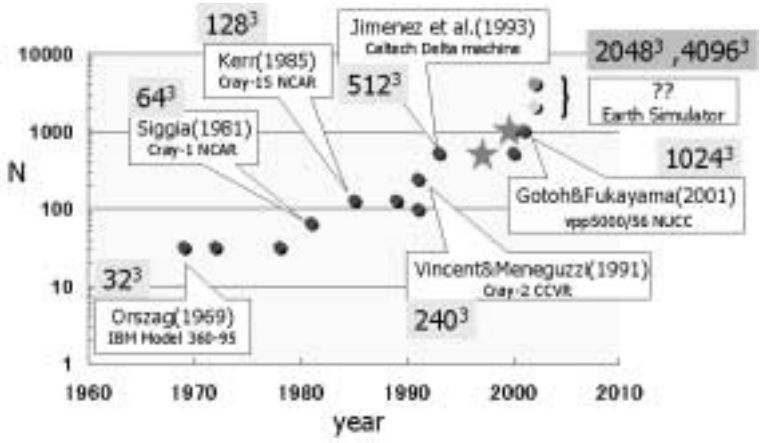


**Fig. 1.** History of DNS of incompressible homogeneous and isotropic turbulence under periodic boundary conditions. Star denotes the position of our DNS.

It is to be recalled here that in DNS of turbulence, the field is generally simulated by solving the equation of motion as an initial value problems. The filed cannot be stationary if there is no external forcing, because turbulence is a dissipative system. Even if there is external forcing, it cannot be stationary in a rigorous sense. If one could continue the simulation for sufficiently long time, then one may expect to realize stationary or quasi-stationary state. However, it is difficult in practice to simulate the DNS for very long time, particularly because the DNS of turbulence is generally quite expensive. This is particularly so in the DNS of turbulence at high Reynolds number in which the number of the degrees of freedom to be solved is enormous. One must stop the DNS at a certain finite time. But little seems to be known, for example, on the effect of the finiteness of the simulation time, how long the initial transient stage is, how strong the effect of non-stationarity is, and so on, in DNS of apparently "stationary" turbulence under external forcing.

In this paper, we report some results of our recent DNS of forced turbulence with the number of grid points up to $1024^3$, where particular attention is paid on the effect of non-stationarity or the transient effect. In the following, we first review the method of our DNS in §2, and then present (1) time series of turbulence characteristics, (2) energy spectrum at a statistically quasi-stationary state, and (3) time series of the energy spectra in §3.

## 2 Numerical method

We consider the motion of an incompressible fluid of unit density which obeys the forced Navier Stokes equations

$$\frac{\partial}{\partial t}\mathbf{u} + (\mathbf{u}\cdot\nabla)\mathbf{u} = -\nabla p + \nu\Delta\mathbf{u} + \mathbf{f}, \tag{1}$$

**Table 1.** DNS parameters and turbulence characteristics at $t = 10$ for Run256 and Run512, and at $t = 5.5$ for Run1024.

| | $R_\lambda$ | $k_{\max}$ | $\Delta t(\times 10^{-3})$ | $\nu(\times 10^{-3})$ | $E$ | $\epsilon$ | $L$ | $\lambda$ | $\eta$ |
|---|---|---|---|---|---|---|---|---|---|
| Run256 | 94 | 121 | 1.0 | 2.0 | 0.5 | 0.0936 | 1.10 | 0.327 | 0.0171 |
| Run512 | 164 | 241 | 1.0 | 0.763 | 0.5 | 0.0811 | 1.26 | 0.217 | 0.00860 |
| Run1024 | 283 | 483 | 0.625 | 0.289 | 0.5 | 0.0727 | 1.21 | 0.141 | 0.00427 |

$$\nabla \cdot \mathbf{u} = 0 \tag{2}$$

under periodic boundary conditions with fundamental periodic box of size $2\pi$ in each direction of the Cartesian coordinates, so that the minimum wavenumber is unity. Here $\mathbf{u}$, $p$, $\nu$, and $\mathbf{f}$ denote velocity, pressure, kinematic viscosity, and external force which satisfies $\nabla \cdot \mathbf{f} = 0$. We solve (1) using an alias-free spectral method for spatial differentiation and a fourth order Runge-Kutta method for time advancing.

A negative viscosity is used to maintain quasi-steady turbulence; in wavenumber space the forcing is given by $\hat{\mathbf{f}}(\mathbf{k}) = -c\hat{\mathbf{u}}(\mathbf{k})$, where $\hat{\mathbf{f}}$ and $\hat{\mathbf{u}}$ are Fourier coefficient of $\mathbf{f}$ and $\mathbf{u}$, respectively, and the value of $c$ is set non-zero only in the wavenumber range $k < 2.5$ and is adjusted every time step so as to keep the total kinematic energy constant ($\langle \mathbf{u} \cdot \mathbf{u} \rangle / 2 = 0.5$). The kinematic viscosity is so chosen that $k_{\max}\eta \sim 2$ in the statistically (quasi-)steady state, where $k_{\max}$ is the maximum wavenumber retained in the simulation and $\eta$ is the Kolmogorov length scale. In our largest DNS (hereafter called Run1024), the number of grid points is $1024^3$ and $k_{\max} = 483$.

Prior to carrying out Run1024, we had performed DNS's with $256^3$ and $512^3$ grid points (hereafter they are referred to as Run256 and Run512, respectively) to study $R_\lambda$-dependence of the turbulence statistics and also to generate initial conditions for the higher-resolution DNS's. The characteristic parameters of the DNS are listed in Table 1. The initial condition for Run256 is a random solenoidal velocity field with the energy spectrum $E(k) \propto k^4 \exp(-k^2/2)$, and the initial fields of Run512 and Run1024 are the same as those of Run256 and Run512 at $t = 10(\sim 5T)$, respectively, where $T$ is the eddy turnover time (see §3 for its definition). The kinematic viscosities of Run 512 and Run1024 are smaller than those of Run256 and Run512, respectively. Run1024 was performed up to $\sim 2.53T$ It took 8,800 time steps.

# 3 Numerical results

## 3.1 Time dependence of one-point statistics

Turbulence can be characterized various statistics. Among them are the so-called one-point statistics or the integrated quantities defined as follows:

the total kinematic energy $E = \frac{1}{2}\langle \mathbf{u}\cdot\mathbf{u}\rangle = \frac{3}{2}u'^2 = \int_0^{k_{\max}} E(k)dk,$

the mean rate of energy dissipation per unit mass $\epsilon = 2\nu \int_0^{k_{\max}} k^2 E(k)dk,$

the integral length scale $L = \frac{\pi}{2u'^2}\int_0^{k_{\max}} k^{-1}E(k)dk,$

the Taylor microscale $\lambda = \left(\frac{15\nu u'^2}{\epsilon}\right)^{1/2},$

the Kolmogorov length scale $\eta = \left(\frac{\nu^3}{\epsilon}\right)^{1/4},$

the eddy turnover time $T = \frac{L}{u'},$

the Kolmogorov time scale $\tau_\eta = \left(\frac{\nu}{\epsilon}\right)^{1/2},$

the Taylor microscale Reynolds number $R_\lambda = \frac{u'\lambda}{\nu},$

the energy dissipation rate scaled on $L$ and $u'$ $a = \frac{\epsilon L}{u'^3}.$

Since the total kinematic energy $E = 3u'^2/2$ is kept constant ($= 0.5$) in our DNS, it follows that (i) $\lambda, \eta, \tau_\eta$, and $R_\lambda$ are completely determined by $\nu$ and $\epsilon$, (ii) $T$ is proportional to $L$, and (iii) $a \equiv \epsilon L/u'^3$ is determined by $\epsilon$ and $L$. These facts suggest that the time dependence/independence of $\epsilon$ and $L$ can be a good measure showing the degree of nonstationarity/stationarity of the simulated field. Note that $\epsilon$ and $L$ depend on the energy spectrum, so that their time dependence reflects that of the energy spectrum. With these in mind, we starts with observing the time dependence of $\epsilon$ and $L$ and then study that of the other one-point statistics, in the following.

Figure 2 shows the evolution of the mean rate of energy dissipation $\epsilon$ per unit mass. It is seen in Fig. 2 that, irrespectively of the differences between the run conditions, all the three curves show that $\epsilon$ increases initially, attains its peak value, and then decreases to attain a local minimum. The curve of Run512 shows that the time dependence of $\epsilon$ after the local minimum is weak, and the other two curves suggest that it is also the case for Run1024 and Run256. The state at which $\epsilon \approx$const. is not realized before the time of the local minimum of $\epsilon$. The time at which $\epsilon$ takes the peak or the local minimum is moved forward in time for DNS with higher resolution. This suggests that the time necessary

for the turbulence to attain its statistically steady state is shorter in DNS with higher Reynolds number.

Fig. 3 shows the time dependence of the integral length scale $L$. Since $u' \sim 1/\sqrt{3}$ in our DNS's, $T$ is obtained by multiplying the values of $L$ in Fig. 3 by $\sqrt{3}$. It is seen that $L$ fluctuate slowly in time around a constant ($\approx 1.2$). Since the main contribution to the value of $L$ is from the energy containing range where an artificial forcing acts, the behavior of $L$ may be directly influenced by the nature of the forcing used in the DNS. Note that the time dependence of $L$ in Run1024 is the weakest among the three runs.

Fig. 4 shows the time dependence of the characteristic length scales $\lambda$ and $\eta$. Since $\lambda \propto \epsilon^{-1/2}$ and $\eta \propto \epsilon^{-1/4}$, the values of $\lambda$ and $\eta$ reflect the time dependence of $\epsilon$. They are seen to be almost constant after the time at which $\epsilon$ takes the local minimum (in that period $\epsilon$ is almost constant).

Fig. 5 shows the time dependence of the length-scale ratios $L/\lambda$ and $\lambda/\eta$. Both the ratios eventually become almost constant, but it is seen that reflecting the behavior of $L$, the ratio $L/\lambda$ varies with time even after the time at which $\epsilon$ takes the local minimum. The ratio $L/\lambda$ is a measure of the width of the inertial subrange. It is seen that $L/\lambda$ is larger for DNS with higher Reynolds number, but $L/\lambda \approx 8$ for Run1024 is still quite small. Fig. 6 shows that the time dependence of the length-scale ratio $L/\eta$ is relatively smaller than that of the time-scale ratio $T/\tau_\eta$, where $T/\tau_\eta$ is given by $T/\tau_\eta = \sqrt{15}L/\lambda$, and $L/\lambda$ is shown in Fig. 5.

Fig. 7 shows that $R_\lambda$ initially decreases and becomes almost constant after the time at which $\epsilon$ takes the local minimum. Note that the value of $R_\lambda$ is relatively high at an initial short transient period, but the ratios, $L/\lambda$ and $T/\tau_\eta$, are smaller than those at the later time. This fact gives a warning that in order to estimate $R_\lambda$-dependence of statistical quantities properly, one need simulate the turbulence field for sufficiently long time, so that a statistically stationarity in the sense $\epsilon \approx$const. is achieved.

Fig. 8 shows the time dependence of $a = \epsilon L/u'^3$. The behavior of $a$ is similar to that of $\epsilon$ in Fig. 2, but even if $\epsilon \approx$const. is approximately satisfied, $a$ fluctuates

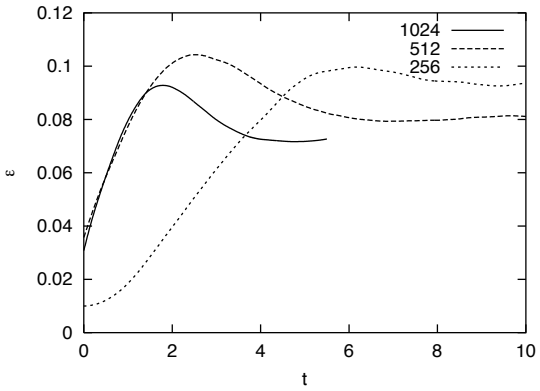


**Fig. 2.** Time dependence of $\epsilon$ in Run1024, Run512 and Run256.

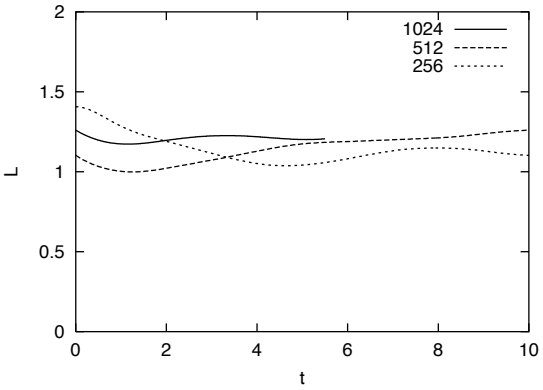


**Fig. 3.** Time dependence of the integral length scale, $L$. The eddy turnover time, $T$, is obtained by multiplying the values of $L$ by $\sqrt{3}$.

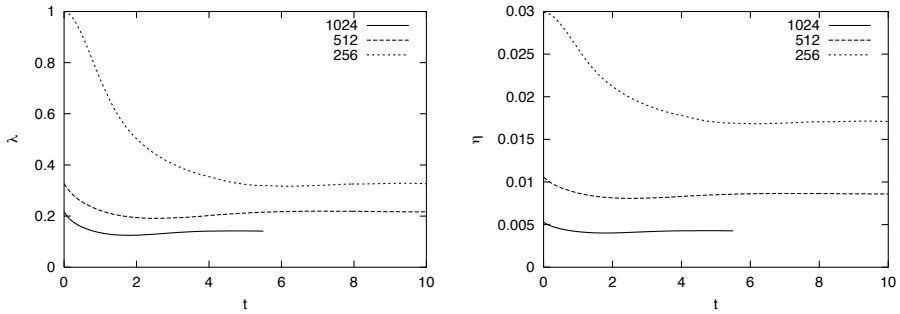


**Fig. 4.** Time dependence of $\lambda$ and $\eta$.

in time due to the fluctuation of $L$ as observed in the curves for Run256 and Run512, in Fig. 3. Therefore the large time-dependence of $L$ makes it difficult to determine the characteristic value of $a$ for the corresponding $R_\lambda$. This suggests that in order to estimate the $R_\lambda$-dependence of $\epsilon L/u'^3$ by DNS, the simulation time need be long enough so as to avoid the effect of the nonstaionarity in the values of $L$ and $\epsilon$. This is particularly true in DNS with lower resolution such as our Run256 and Run512. Since the variance of $L$ is relatively small for Run1024, it is easier to determine the characteristic value of $a$ for $R_\lambda = 283$.

In Fig. 9, we plot, as a function of $R_\lambda$, the first minimum value of $\epsilon L/u'^3$ after $\epsilon L/u'^3$ attains its peak value, and compare the results with recent data from Gotoh *et al.* [8] as well as previous DNS data [6,8–11], which are listed in Ref. [12]. The data, especially those from our DNS and Gotoh *et al.*[8], suggest that $\epsilon L/u'^3$ approaches to a constant with the increase of $R_\lambda$, and it is almost constant ($= 0.44 - 0.45$) for $R_\lambda > 280$ or so. The consideration in the above paragraph suggests that the data for $R_\lambda < 200$ are scattered presumably because of insufficient length of simulation time.

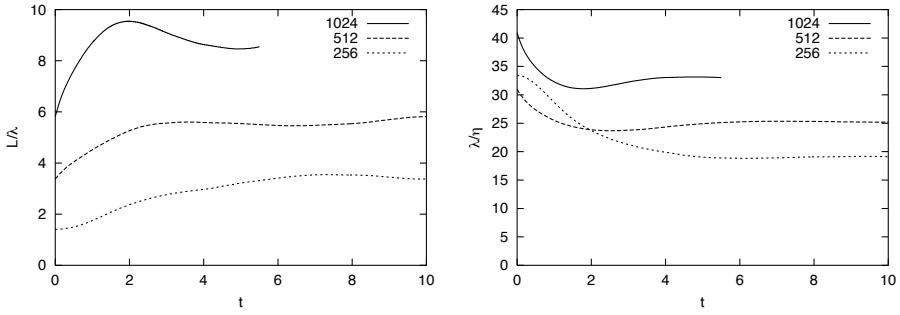


**Fig. 5.** Time dependence of the ratios $L/\lambda$ and $\lambda/\eta$.

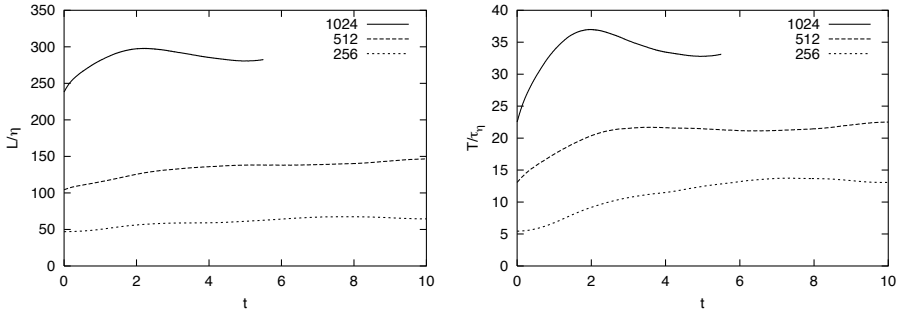


**Fig. 6.** Time dependence of the ratios $L/\eta$ and $T/\tau_\eta$.

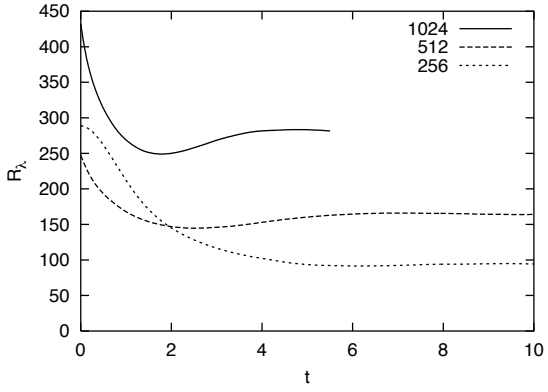


**Fig. 7.** Time dependence of $R_\lambda$.

It may be interesting to note here that
(i) in spite of the similarity of our forcing to that of Jimenez *et al.*[6], the values of $\epsilon L/u'^3$ for $R_\lambda < 200$ are different from each other; $\epsilon L/u'^3 = 0.49 - 0.57$ for

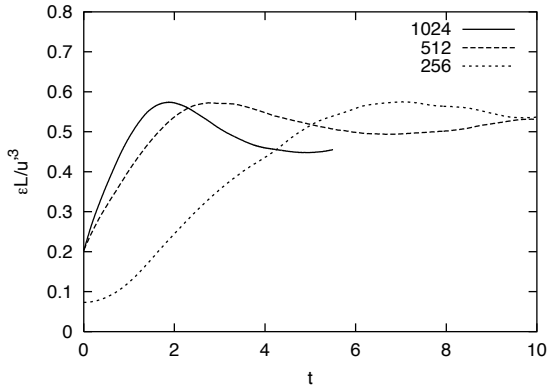


**Fig. 8.** Time dependence of the normalized rate of energy dissipation $\epsilon L/u'^3$.

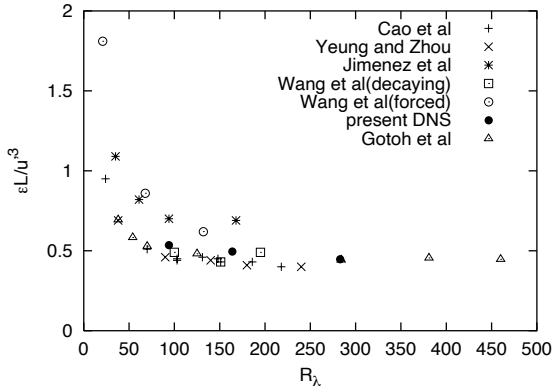


**Fig. 9.** $\epsilon L/u'^3$ vs. $R_\lambda$.

$R_\lambda = 164$ in our DNS, while $\epsilon L/u'^3 = 0.69$ for $R_\lambda = 168$ in DNS by Jimenez *et al.*,
(ii) on the other hand, in spite of the difference between our forcing and that in Gotoh *et al.*[8], the values of $\epsilon L/u'^3$ are almost the same to each other for $R_\lambda > 280$; $\epsilon L/u'^3 = 0.447$ for $R_\lambda = 283$ in our DNS, while $\epsilon L/u'^3 = 0.442$ for $R_\lambda = 284$ in the DNS by Gotoh *et al.*.

### 3.2 Energy spectrum at a statistically quasi-stationary state

Figure 10 shows the normalized energy spectra

$$\epsilon^{-1/4}\nu^{-5/4}E(k)$$

obtained from snapshots of Run256 ($t = 10$), Run512 ($t = 10$), and Run1024 ($t = 5.5$), as functions of the normalized wavenumber $k\eta$. It can be seen that

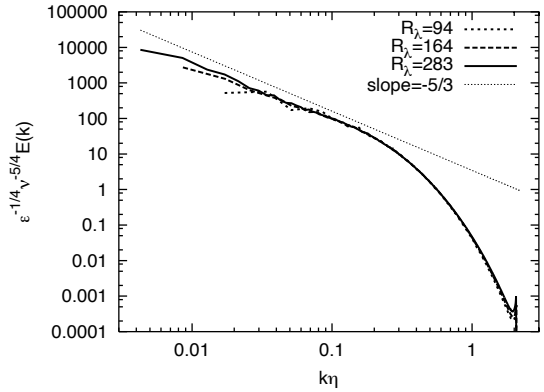


**Fig. 10.** Normalized energy spectrum $\epsilon^{-1/4}\nu^{-5/4}E(k)$ at $t = 10$ of Run256 and Run512, and at $t = 5.5$ of Run1024.

irrespectively of $R_\lambda$ the normalized energy spectra overlap each other at high wavenumbers.

Figure 11 and 12 respectively show the comparisons of the compensated energy spectrum defined by

$$\epsilon^{-2/3}k^{5/3}E(k)$$

and normalized energy flux defined by

$$\frac{\Pi(k)}{\epsilon} = \frac{1}{\epsilon}\int_k^\infty T(k')dk',$$

at different $R_\lambda$, where $T(k)$ is the energy transfer function. These plots are obtained from the same fields as in Fig. 10. In contrast to Fig.10, the difference between the three spectra is clearly visible in Fig.11.

Figure 12 shows that there exists a plateau, at $k\eta \approx 0.06$ for $R_\lambda = 94$, at $0.02 < k\eta < 0.07$ for $R_\lambda = 167$ and at $0.01 < k\eta < 0.06$ for $R_\lambda = 283$, where $\Pi(k)$ is nearly independent of $k$. It is seen that the value of $\Pi(k)$ at the plateau agrees well with the value of $\epsilon$ for $R_\lambda = 283$, while the agreement is not so good for $R_\lambda = 94$ and 164.

In Fig. 11, $k^{5/3}E(k)/\epsilon^{2/3}$ is seen to be nearly constant in the plateau range for the case of $R_\lambda = 283$. On the other hand, the plateau range of $\Pi(k)$ for $R_\lambda = 94$ and 164 is very small, and it is difficult to find in Fig. 11 a scaling range, where the compensated energy spectrum is constant independent of $k$. In Fig. 11, we can also observe bumps, each of which has a peak at $k\eta \approx 0.15$ irrespectively of $R_\lambda$. This kind of bump has been also observed in experiments, e.g. [13]. Note that the bump is at the wavenumber range $k\eta > 0.07$, where $\Pi(k)$ is a decreasing function of $k$, and the inertial subrange lies in $k\eta < 0.07$. This fact suggests that in order to obtain an inertial subrange we have to resolve modes with wavenumbers much smaller than $k\eta \approx 0.07$.

The Kolmogorov constant $C_K$ defined by

$$E(k) = C_K\epsilon^{2/3}k^{-5/3} \tag{3}$$

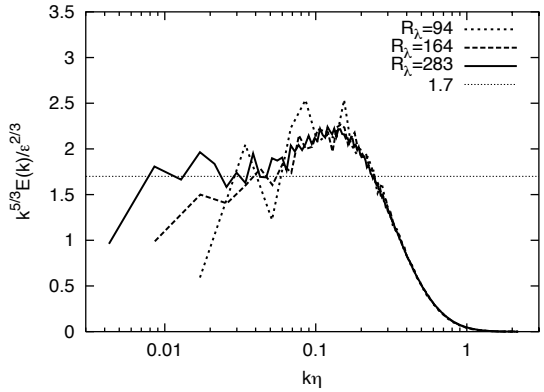


**Fig. 11.** Compensated energy spectrum $\epsilon^{-2/3}k^{5/3}E(k)$ at $t = 10$ of Run256 and Run512, and at $t = 5.5$ of Run1024.

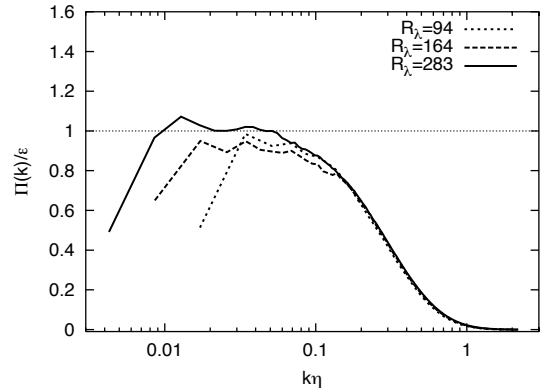


**Fig. 12.** Normalized energy flux $\Pi(k)/\epsilon$ at $t = 10$ of Run256 and Run512, and at $t = 5.5$ of Run1024. The dotted straight line denotes $\Pi(k)/\epsilon = 1$.

in the inertial subrange can be estimated from the plot for $R_\lambda = 283$ at $0.01 < k\eta < 0.06$ in Fig. 11. We then obtain $C_K \approx 1.7$. This value 1.7 is consistent with previous experiments [14], spectral closure theories [15,16] and recent numerical simulations, [10,8] whose forcing scheme and the value of $k_{\max}\eta(\approx 1)$ are different from those in our DNS. These suggest that the Kolmogorov constant of the inertial subrange are insensitive to the detail of such flow conditions as forcing at large scale and wavenumber truncation at small scale. However it is also to be remembered that some statistical quantities such as high order structure functions in the inertial subrange are sensitive to the value of $k_{\max}\eta$ (see analysis in Ref. [17]).

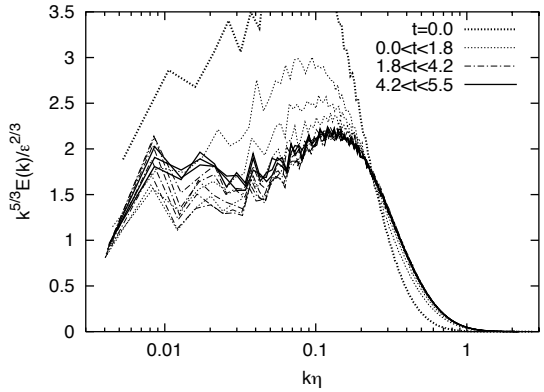


**Fig. 13.** Time series of compensated energy spectrum $\epsilon^{-2/3}k^{5/3}E(k)$ in Run1024.

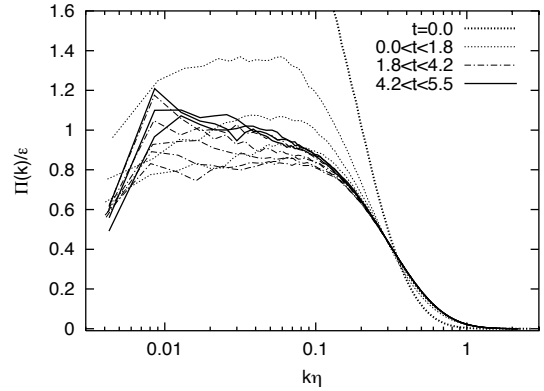


**Fig. 14.** Time series of normalized energy flux $\Pi(k)/\epsilon$ in Run1024.

### 3.3 Time dependence of the energy spectrum

In the present DNS, the total energy $E$ is kept constant so that the behavior of $\epsilon$ and $L$ determines that of the other one-point statistics discussed in §3.1. It was shown in §3.1 that (i) $L$ depends on time, but its dependence is weak, and (ii) the time dependence of $L$ is weaker for larger $R_\lambda$. Therefore we study here the time dependence of spectra in the DNS with the highest $R_\lambda$, i.e., Run1024, with taking account of the time dependence of $\epsilon$. Regarding the evolution of $\epsilon$, it was seen in Fig.2 that there are at least three characteristic stages;
(i) for $0.0 < t < 1.8$, $\epsilon$ increases sharply with $t$,
(ii) for $1.8 < t < 4.2$, $\epsilon$ decreases gradually, and
(iii) for $4.2 < t$, $\epsilon$ is almost constant.

Figures 13 and 14 respectively show the compensated energy spectrum and the energy flux function normalized by $\epsilon$ at various times from Run1024. It can be seen in Fig. 13 that in the stage (i) the compensated spectrum as well as the

normalize energy flux are not stationary in the entire wavenumber range, while in the stage (ii) and (iii) ( $t > 1.8$), the energy spectra at $k\eta > 0.1$ agree well with each other and at the stage (iii) ($t > 4.2$), the energy spectra at $0.02 < k\eta < 0.06$ are close to 1.7. It is seen in Fig. 14 that in the stage (ii), the values of $\Pi(k)/\epsilon$ at $k\eta > 0.1$ agree well with each other and in the stage (iii), the values of $\Pi(k)/\epsilon$ at $0.02 < k\eta < 0.06$ are close to 1.0. These observations suggest that the turbulent velocity field by Run1024 ($R_\lambda = 283$) attains its quasi-statistically steady state (at least, regarding the energy spectrum and the energy flux) and exhibits an equilibrium inertial subrange with the $k^{-5/3}$ energy spectrum after $t = 4.2(\approx 2T)$. One needs to be careful not to misread the energy spectra at the transient stage before that period to be an equilibrium one; the confusion might then result in, for example, an overestimate of the Kolmogorov constant.

## 4 Acknowledgement

The authors are grateful to Professor K. R. Sreenivasan for stimulating discussions which encourage our making plots in Fig. 9. This work was supported by "Research for the Future" Program of the Japan Society for the Promotion of Science under the project JSPS-RFTF97P01101.

## References

1. A. N. Kolmogorov: Dokl. Akad. Nauk SSSR **30** 9 (1941)
2. S. A. Orszag: Phys. Fluids, **12** II-250 (1969)
3. E. D. Siggia: J. Fluid Mech. **107** 375 (1981)
4. R. M. Kerr: J. Fluid Mech. **153** 31 (1985)
5. A. Vincent, M. Meneguzzi; J. Fluid Mech. **225** 1 (1991)
6. J. Jimenez, A. A. Wray, P. G. Saffman, R. S. Rogallo:J. Fluid Mech. **255** 65 (1993)
7. T. Gotoh, D. Fukayama: Phys. Rev. Lett. **86** 3775 (2001)
8. T. Gotoh, D. Fukayama, T. Nakano: Phys. Fluids **14**, 1065 (2002)
9. N. Cao, S. Chen, G. D. Doolen: Phys. Fluids **11** 2235 (1999)
10. P. K. Yeung, Y. Zhou: Phys. Rev. E **56**, 1746 (1997)
11. L. P. Wang, S. Chen, J. G. Brasseur, J. C. Wyngaard: J. Fluid Mech. **309**, 113 (1996)
12. K. R. Sreenivasan: Phys. Fluids **10**, 528 (1998)
13. K. R. Saddoughi, S. V. Veeravalli: J. Fluid Mech. **268**, 333 (1994)
14. K. R. Sreenivasan: Phys. Fluids **7**, 2778 (1995)
15. R. H. Kraichnan: Phys. Fluids **8**, 575 (1965)
16. Y. Kaneda: J. Fluid Mech. **107**, 131 (1981)
17. Y. Yamazaki, T. Ishihara, Y. Kaneda: J. Phys. Soc. Jpn. **71**, 777 (2002)